

Research Article

3D S-Wave Velocity Model of the Crust and Upper Mantle beneath the Sea of Okhotsk and the Kamchatka Peninsula

Victor Corchete 

Higher Polytechnic School, University of Almeria, 04120 Almeria, Spain

Correspondence should be addressed to Victor Corchete; corchete@ual.es

Received 31 December 2021; Accepted 28 May 2022; Published 15 June 2022

Academic Editor: Feng Cheng

Copyright © 2022 Victor Corchete. Exclusive Licensee GeoScienceWorld. Distributed under a Creative Commons Attribution License (CC BY 4.0).

A 3D S-wave velocity model (from 0 to 350 km depth) is determined for the region of the Sea of Okhotsk and the Kamchatka peninsula, through Rayleigh wave analysis applied to the traces of 278 earthquakes registered by 12 seismic stations, both located within (and nearby) of the study area. This model reveals the principal geological and tectonics features present in the study area, e.g., the presence of two lower-crust hot plumes located at the northwest of the Sea of Okhotsk, which are shown as two zones of low S-wave velocity (from 20 to 30 km depth). Also, a conspicuous low S-wave velocity zone is determined at the southwest of the Sea of Okhotsk (from 35 to 60 km depth), which can be matched up with a high conductivity layer previously determined from 30 to 65 km depth. For the Kamchatka peninsula, low S-velocities are determined beneath the volcanic belt from the upper crust (~5 km-depth) down to a depth of ~60 for the southern part, and down to a depth of ~140 km for the northern part. This low S-wave velocity pattern is enlarged in size at the northwest (north of ~55°N), following the location of the Kliuchevskoi and Sheveluch volcanoes, which confirms that these volcanoes must be a part of the same subduction-induced volcanic process. The present model shows that the subducting Pacific slab terminates near to the Aleutian-Kamchatka junction, i.e., no relict slab underlies the extinct northern Kamchatka volcanic arc. This model shows that this slab shoals towards north, and there exists a gap associated with the loss of this slab beneath Sheveluch and Kliuchevskoi volcanoes. The low S-wave velocity pattern determined at northwest of the slab edge confirms the presence of the asthenospheric flow, which would pass through this gap to the northwest around the north slab edge. Finally, the present model shows the precise location and detailed structure of the asthenosphere, which is a new result that has not been determined in other previous studies.

1. Introduction

Several surface wave studies of the crust and upper mantle structure have been conducted for the present study area: Sea of Okhotsk and the Kamchatka peninsula [1–7]. Unfortunately, the majority of these studies have a grid spacing relatively large (ranging from 5° to 8° and even degrades at periods above 100 s or near the periphery of the maps) to show fine details of this structure, for a relatively small area as considered in the present study (Supplement 1a). However, some of these previous studies have a grid spacing relatively short and adequate to give fine details of this structure, and they are local and short-scale studies limited to the crust (or limited to the very shallow upper mantle). These studies have no information about the lithosphere

and asthenosphere structure. For all that, a new 3D S-wave velocity model is needed with the maxima resolution and depth possible (i.e., with the resolution and depth increased as much as possible), which can give the desired fine details (i.e., with a resolution of ~1°) of the crust and upper mantle structure (i.e., lithosphere and asthenosphere structure) for the present study area, and this is the goal of the present study. As the maximum resolvable resolution of a model is determined by the data and methods, in the present study, this resolution will be achieved considering the path coverage of the Rayleigh waves within (and nearby) of the study area, with the maxima depth possible (from 0 to 350 km depth) considering the wider period range possible (from 5 to 175 s), and using the methods described in Section 3, which have been proved as a very efficient methodology in

many similar previous studies (e.g., [8]). On the other hand, many studies of the crust and upper mantle structure has been developed for the present study area concerning P-wave velocities (e.g., [9–14]), while only a few studies concerning S-velocities have been performed for the same area. However, the knowledge of the S-wave velocity structure is essential in many practical items, e.g., in the estimation of the ground motions for future earthquakes, or the improvement of the earthquake locations and the estimation of their focal parameters. For these practical issues, this new model can provide a valuable help. This new model also can help to understand the complicated structures of the crust and upper mantle that exist in East Asia and West Pacific marginal sea, from which the present study area is an important part. Those complicated structures are related to the dynamic processes of deep earth occurred from Mesozoic (~150 Ma). This new model will complete the 3D S-wave velocity models performed by Corchete [8, 15] for East Asia and West Pacific marginal seas. Consequently, this model joint to those determined by Corchete [8, 15] will be a very important tool to understand the relationships between the surface tectonics and the deep earth's structures, and thus to understand the evolution of this region.

2. Geological Setting

The present study area comprises the Sea of Okhotsk and the Kamchatka peninsula. The Sea of Okhotsk (SO) is bounded on the north and northwest by the eastern Russia (RU), on the east by Sakhalin (SA), on the west by the Kamchatka peninsula (KP), and on the south by the Kuril trench (KT), as shown in Figure 1. The SO and the KP can be considered parts of the same plate [16]. They examined several well-constrained focal mechanisms of events occurred in northeastern Siberia, to determine the nature of the North American plate boundary in the northeastern part of Siberia, concluding that an independent plate exists. They concluded that the Suntar-Khayata Mountains, the southwestern Cherskii Mountains, the east-middle of SA, the northern part of Hokkaido Island, the SO and the major southern part of the KP lie on a common plate: the Okhotsk plate [17, 18]. The existence of this plate was confirmed by the slip vectors determined from the earthquake focal mechanisms by Seno et al. [19] and evidenced in more recent studies developed in this area (e.g. [10, 13, 20–24]).

The SO is considered a part of the Neozoic marginal basins called the Cenozoic marginal sea basin with ~8000 km-length and 2500-4000 km-width; from the SO, the Kuril basin (KB), the Sea of Japan, North China-South China and the South China Sea to the Philippine Sea [6, 7]. The KB is defined by the contour line of 3000 m isobath in Figure 1 [25]. This block is characterized by thin lithosphere (50-100 km thick), thick asthenosphere (100-200 km-thick) and a low seismic velocity belt located in the upper mantle [8, 15]. The low-velocity belt is associated to the East Asian rifting system, which is evidenced by many geological and geophysical characteristics, e.g., anomalies in the lithospheric density distribution or temperature differences within the lithosphere (e. g., [6, 7, 26, 27]). The litho-

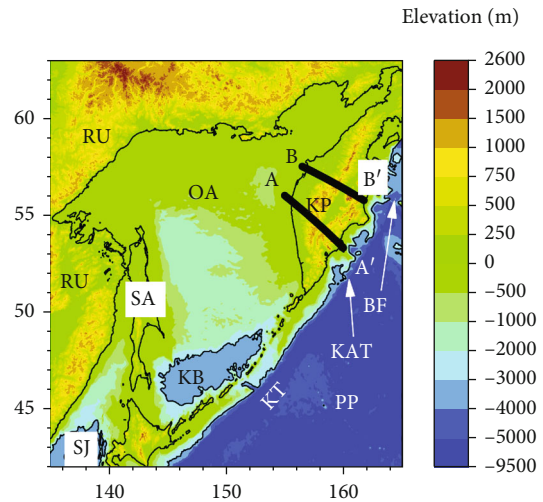


FIGURE 1: Elevation map of the study area [7, 28]. The used abbreviations are as follows: BF: Bering fault; KB: Kuril basin; KAT: Kamchatka trench; KT: Kuril trench; KP: Kamchatka peninsula; OA: Okhotsk Arch, PP: Pacific plate, RU: Russia; SA: Sakhalin; SJ: Sea of Japan. The 3000 m isobath is plotted with black thin line. The lines AA' and BB' denotes the location of the NW-SE profiles displayed in Figure 4.

osphere thinning (and its corresponding asthenosphere thickening) was caused by the asthenospheric material upwelling since Mesozoic (~150 Ma), and the continental margin continued to develop large-scale rifts and marginal seas in Cenozoic [6]. The Pacific plate is subducting beneath SO at the Kuril trench (Figure 1) and its dip angle becomes gradually smaller from north (45°-50°, southern Kamchatka) to south (30°, northern Japan) beneath the Kuril arc [28].

The SO is considered by Zeng and Lay [29] as an exotic terrane without a clear tectonic history defined, which is characterized by an intermediate thick crust (19-24 km thick), except for the KB, and an anomalous upper mantle (with thin lithosphere). According to Christensen and Mooney [30] a thin continental crust may overlay a weak and thin lithosphere, and probably this crust is thickened by subcrustal flow. However, Zeng and Lay [29] consider that it is unclear whether the SO crust is continuing to thicken by deformation or underplating. The SO consists of deformed Cretaceous and Mesozoic (and, perhaps, Upper Paleozoic) geosynclinal formations [25, 31]. In some outcrops of the Okhotsk Arch the basement may be probably older than Paleozoic [31]. The KB has the thinnest crust of the SO with a thickness of ~10 km, as shown by the studies on the deep structure developed for this region [25, 31–34]. The deep water basins, as the KB, generally are assumed to have an oceanic-type crust [35], because it is commonly accepted that the oceanic crust is a thin crust (<10 km thick, in general).

The Kamchatka peninsula (KP, Figure 1) is located at the east of the present study area, and its tectonic regime is principally determined by the subduction of the PP under the Eurasian plate. The PP is subducting beneath the KP at

the Kamchatka trench (KAT, Figure 1) and moving along the strike-slip Bering fault (BF, Figure 1, [36, 37]). In this peninsula, a chain of active volcanoes (Holocene in age) along its eastern coast are underlain by the subducting Pacific slab at ~100 km-depth [14, 38]. The depth of this slab is defined to a maximum of ~500 km in the southern part of the Kamchatka, and this depth shoals gradually to ~300 km towards the north [9, 12, 38]. The dip angle of this slab is ~55° from ~50°N to ~54°N, but a drastic change in the dip angle is observed north of ~54°N, near the Aleutian-Kamchatka junction [9]. North of ~54°N, this slab is sharply deformed and becomes shallower at ~100 km depth [9]. This drastic change in dip angle (and its corresponding abrupt shallowing of the slab) may occur in younger subduction environments such as Peru or Mexico [39, 40], but in Kamchatka, it takes place in one of the oldest subducted slabs in the world [41]. This controversy can be solved presenting some model to explain this conspicuous feature, and two models have been presented. The first model, proposed by Levin et al. [42], suggests that a relic slab detached from the westward subduction of the Pacific plate 2 Ma ago, but their model does not show how the slab is separated and where the relic slab is. The second model, proposed by Jiang et al. [11], suggests that a gap exists in the subducting slab (near the Aleutian-Kamchatka junction), and it is associated with the loss of the slab beneath Kliuchevskoi and Sheveluch volcanoes, near the northern Pacific slab edge. Then, the asthenospheric flow can pass through this gap (and around the slab edge) to the north. The existence of this slab gap is also suggested by Yogodzinski et al. [43], who located this slab window beneath the western Aleutian and the Aleutian-Kamchatka junction, and suggested that the mantle flow (asthenospheric flow) can pass through this window from the Aleutian arc into the Kamchatka peninsula, which may induce the partial melt to the slab edge in the overlying mantle [44]. Also, shear-wave splitting studies [45, 46] indicate that the asthenospheric flow passes through a slab window beneath the junction, similar to that observed in Apennines [47]. In the model proposed by Jiang et al. [11], it is observed that the loss of slab mainly occurred near to the Meiji seamounts. Davaille and Lees [48] suggested that the presence of the Meiji seamounts can accelerate the partial melt of the slab in the north. Thus, the thermal friction originated by the mantle flow (asthenospheric flow) and the Meiji seamounts jointly cause the diminishment of slab near its edge, i.e., the slab near the edge is thinner than that under southern Kamchatka, because the Meiji Seamounts subducting together with the Pacific plate. This model is consistent with the results presented by Lees et al. [12]. On the other hand, this abrupt shallowing of the subducted slab has produced that the Kliuchevskoi and Sheveluch volcanoes have shifted north-westward from the volcanic front [9, 11, 49]. All the above indicates that the seismic velocity structure that could be determined for the KP is expected to be very complex, due to the presence of a subducting slab (sharply deformed north of 54°N), an active volcanic belt, a deep trench (KAT, Figure 1), and thick sedimentary basins in the Central Kamchatsky graben [9].

3. Data and Methodology

The dataset used in the present study has been the traces of 278 earthquakes (Supplement 1) registered by 12 seismic stations (Supplement 2). These earthquakes were grouped in source zones (Supplement 3). Thus, the earthquakes with very similar coordinates (differences < 1°) are grouped in the same source zone [50]. Also, some stations show very similar coordinates (differences < 1°), and these stations were grouped in averaged stations (Supplement 4). The Rayleigh wave fundamental-mode group velocities (i.e., the dispersion curves) was determined for the trace of each event (Supplement 1) registered by each station (Supplement 2), by means of digital filtering techniques [50]. An example of this process is shown in Supplements 5 to 8. These dispersion curves were averaged by source zones and stations to calculate the dispersion curves corresponding to the source-station paths [50], which path coverage is shown in Supplement 9a, with periods ranging from 5 to 175 s (Supplement 9b). In Supplement 10, the values of these group velocities are presented for several periods. These source station dispersion curves were regionalized to calculate the regional group velocity $U(x, y)$, where x is the longitude and y is the latitude. $U(x, y)$ is a continuous function defined over the area covered by the paths [51]. The values of $U(x, y)$ and its 1-sigma error are shown in Supplements 11 and 12, respectively. These group velocities $U(x, y)$ calculated for each period, from 5 to 175 s, are sampled in rectangular grids of $1.25^\circ E \times 0.75^\circ N$ mesh size to perform their inversion process, following the inversion method detailed by Corchete et al. [50]. These grid points are the centers of a grid with rectangular blocks [52]. These grid data are then inverted obtaining a shear velocity model (a shear velocity distribution with depth) for each grid point (or block) of the study area, achieving thus a 3-D S-velocity model. In this inversion procedure, the good selection of an initial earth model is a previous important step before the inversion process [50]. This initial model must represent all the information available for the study area, respect to the S-wave, P-wave, and density distributions with depth (see above in the geological setting of this paper). In Supplement 13 is listed the initial model prepared for the example of inversion shown in Supplement 14. For depths greater than 300 km, the preliminary reference earth model developed by Dziewonski and Anderson [53] has been used. On the other hand, an adequate layer thickness (depth intervals in Supplement 15) must be selected to improve the solution reliability of the inversion process (i.e., to achieve the better resolution). The number of layers (depth intervals) considered in the earth model (S-velocity model) must be reduced to the minimum, which are necessary to obtain a detailed S-velocity distribution with depth, as required to satisfy the observed dispersion data (the regionalized group velocities). Corchete et al. [50] proved that the selection of smaller layer thicknesses (e.g., 1 or 2 km), with a larger number of layers, gives a bad resolution. A bad resolution implies the existence of many similar models (most of them are absurd or meaningless models), which can fit the observations (group velocities). As an example of the inversion process performed in the present

study, Supplement 14 shows the obtained results for the inversion of the dispersion curve for the block area located at the coordinates: 55.375°N, 158.125°E. It should be noted that the S-velocity models (Supplement 14a) and the resolving kernels (Supplement 14b) are plotted only for depths above 800 km. This fact is due to the poor resolution obtained for depths greater than 350 km (Supplement 14b). Therefore, the results obtained for depths below 350 km have been omitted. The abovedescribed S-velocity distributions with depth, obtained for each grid point (or rectangular block) of the abovementioned grid defined in the study area, are plotted in contour maps as shown in Supplement 15 (and Figure 2). The 1-sigma errors and the lateral resolution of these S-velocities (Supplement 15) are shown in Supplements 16 and 17, for several depths. The resolution maps of Supplement 17 are estimated from the resolving kernels (e.g., Supplement 14b) calculated in the inversion process, which is performed for the dispersion curve associated to each grid point: the value of each resolving kernel at its reference depth is annotated to be plotted later in a resolution map, as is shown in Supplement 17. The reference depths are the media depth of the layers considered in the inversion process, and their resolution values (resolving kernel values at the reference depths) can vary from 0 (not resolved) to 1 (perfect resolution). Finally, in Figure 3, the principal vertical discontinuities present in the earth structure beneath the study area are shown, determined from the 3D S-wave velocity model [52]: the Moho discontinuity, the lithosphere-asthenosphere boundary (LAB), and the asthenosphere base boundary (ABB). The Moho map (Figure 3(a)) has been calculated considering, for each grid point of the study area, the first depth in which the S-velocity value jumps above 4 km/s, i.e., the S-velocities greater than 4 km/s have been associated to the mantle. This surface has been considered as the Moho boundary. The map of the LAB (Figure 3(b)) has been computed considering the depth in which the S-velocity starts to decrease with depth, below the Moho discontinuity. The map of the ABB (Figure 3(c)) has been computed similarly, but now considering the depth in which the S-velocity starts to increase below the LAB. The S-wave velocity in which these decreasing and increasing occur has the value 4.4 km/s, in the present study. Thus, the asthenosphere is defined, as a low S-wave velocity channel in the upper mantle, with S-wave velocity values lower than 4.4 km/s. In general, the S velocities in the asthenosphere are ~4.3 km/s. Nevertheless, these values can be lower than 4.3 km/s in areas that present asthenospheric flow (Figure 4), where the asthenosphere materials are very hot and partially melted.

4. Results

4.1. Depth Range: 0-5 km. In Supplement 15, a prominent low S-wave velocity zone (~2.1 km/s) is shown in the KP for the Central Kamchatsky graben, and in the SO for the KB. Also, lower S-wave velocity values (2.1-2.2 km/s) are determined for the SO.

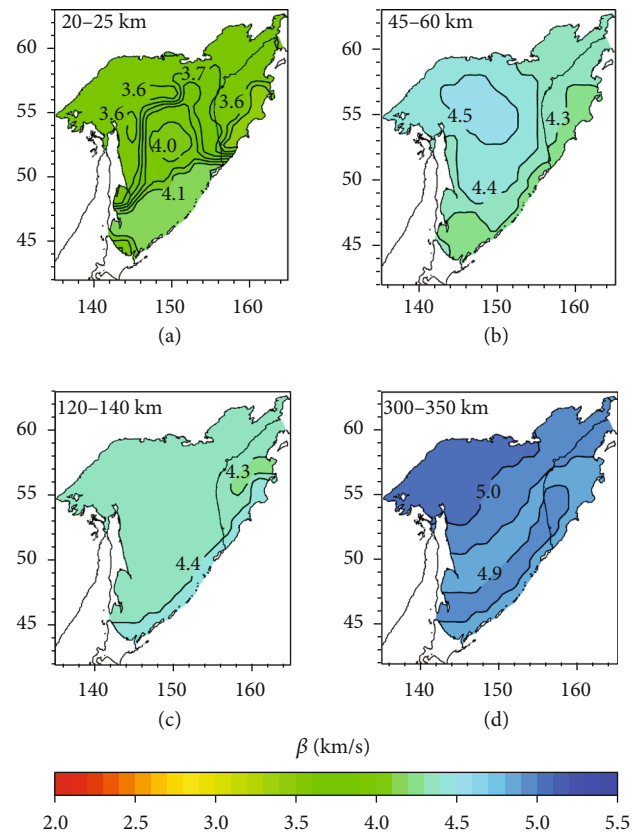


FIGURE 2: Geographical distribution of the S-wave velocity as a function of depth. The interval between isolines is 0.1 km/s.

4.2. Depth Range: 5-35 km. Low S velocities (~3.6 km/s, Figure 2(a)) are determined at the northwest of the SO, in the depth range from 20 to 30 km (Supplement 15), approximately. Also, low S velocities (Figure 2(a)) are determined beneath the volcanic belt of the KP [54], for both upper and lower crusts (Supplement 15). On the other hand, high S velocities (Figure 2(a) and Supplement 15) are determined for the regions with thinner crustal thickness (Figure 3(a)), because the S-wave velocity values are influenced by the presence of the near mantle. For the SO, the crustal thickness varies from ~10 km beneath the KB to ~30 km near to SA (Figures 1 and 3(a)).

4.3. Depth Range: 35-60 km. For the SO, its older regions [31] present the higher S-wave velocity (Figure 2(b)), which is more evident for the Okhotsk Arch (OA, Figure 1). A conspicuous low S-wave velocity is determined at the southwest (Figure 2(b) and Supplement 15). Also, low S-velocities are determined near to the Kuril arc and along it (Figure 2(b)). For the KP, low S-velocities are determined beneath the volcanic belt (Figures 2(a) and 2(b)), in the same area as in the previous depth range (5-35 km depth). This low S-wave velocity pattern is enlarged in size at the northwest, north of ~55°N (Figures 2(b), 2(c), and 4), following the location of the Kliuchevskoi and Sheveluch volcanoes [9].

4.4. Depth Range: 60-240 km. The asthenosphere is mapped as low S velocities (~4.3 km/s) versus depth (Figure 2(c))

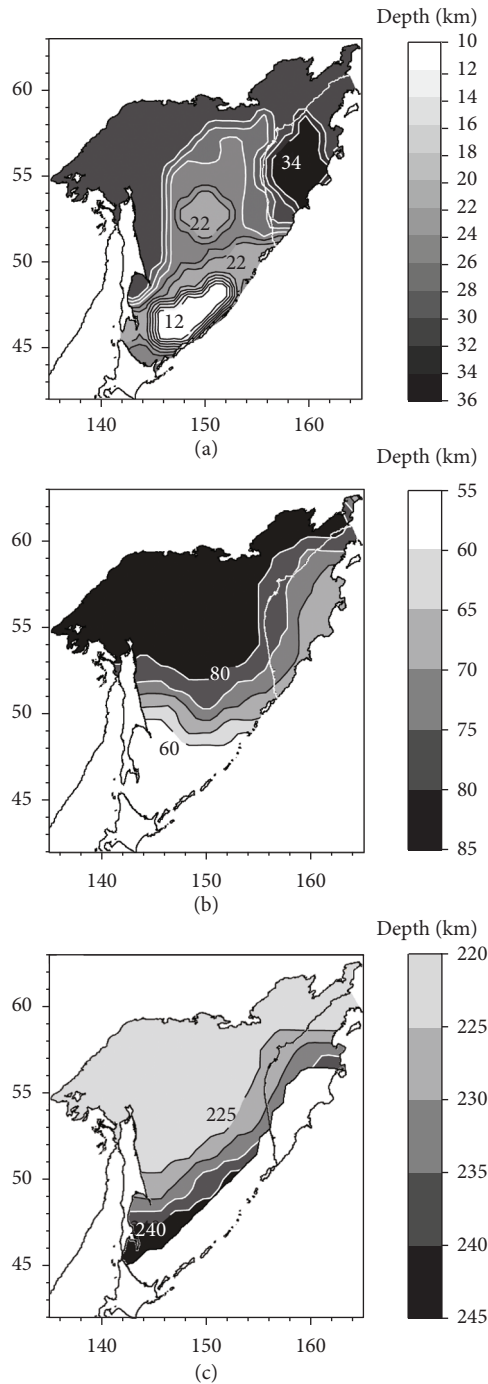


FIGURE 3: Map of the Moho discontinuity (a), the lithosphere-asthenosphere boundary (b), and the base of the asthenosphere (c). The interval between isolines is 2 km for Figure 3(a) and 5 km for Figures 3(b) and 3(c). The white color is used in Figure 3(c) to show the high S-wave velocity zone associated to Pacific slab, in which no low-velocity channel (asthenosphere) can exist and no ABB can be defined.

and Supplement 15), between the LAB and the ABB (Figures 3(b) and 3(c), respectively). The precise location and detailed structure of the asthenosphere determined in the present study are a new feature that has not been determined in other previous studies. On the other hand, the tec-

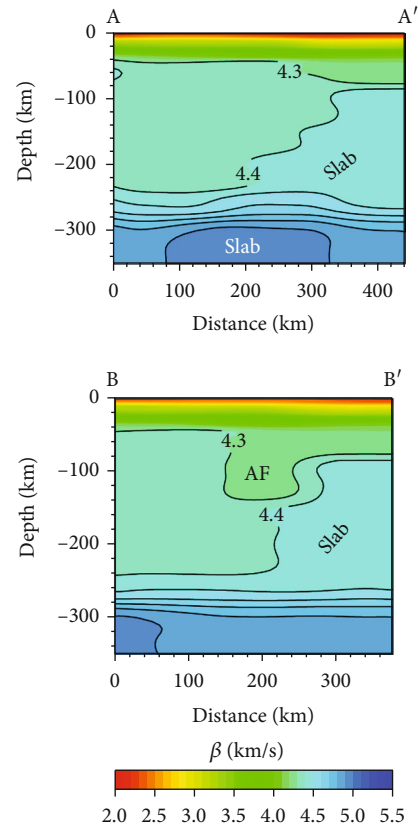


FIGURE 4: S-wave velocity structure along the NW-SE profiles shown in Figure 1 (obtained from the 3D S-wave velocity model shown in Figure 2 and Supplement 15). The interval between isolines is 0.1 km/s. The abbreviation AF denotes asthenospheric flow.

tonic features of the subduction zones are clearly visible in terms of S-velocities (Figures 2(b)–2(d)), i.e., the subducting Pacific slab is shown as a high S-wave velocity pattern, and its corresponding wedge (above this slab) is shown as a low S-wave velocity pattern (Figure 4).

4.5. Depth Range: 240–350 km. For the SO, the high S-wave velocity area (Figures 2(c) and 2(d)) near to the Kuril arc increased in size gradually, from north to south. For the KP, the S-wave velocity mapping (Figures 2(c), 2(d), and 4) shows that the subducting slab (Pacific lithosphere) terminates near to the Aleutian-Kamchatka junction. Also, the S-wave velocity mapping (Figure 4 and Supplement 15) shows that this slab shoals towards north. In the profile BB' shown in Figure 4, no high S-wave velocity associated to this slab is determined for depths greater than 240 km, and a low S-wave velocity pattern is determined northwest of the slab edge (Figures 2(b) and 2(c) and profile BB' of Figure 4).

5. Interpretation and Discussion

5.1. Depth Range: 0–5 km. The prominent low S-wave velocity zone shown for the Central Kamchatsky graben could be associated to the large sedimentary basins present in this

area, with thicknesses of up to 5 km [9, 55, 56]. Also, the low S velocities determined for the KB could be related to the thick (>4 km) sedimentary beds present in this area [25]. This thick cover of sediments is unusual for an oceanic basin, as the KB [35, 57–59]. In general, the SO shows lower S-wave velocity values that may be related with the thicker sedimentary cover present in this region. The thickness of this sedimentary cover ranges from 0.2 to 0.5 km, but it can reach more than 5–6 km in the basement troughs [31, 60, 61].

5.2. Depth Range: 5–35 km. The low S-wave velocity pattern determined at the northwest of the SO, in the depth range from 20 to 30 km (Supplement 15), is clearly associated to the presence of two lower-crust hot plumes in this area [62]. The presence of these features in the crust is very unusual, the plumes are observed in the upper mantle, generally. Nevertheless, the abovementioned low S-wave velocity pattern evidences the presence of two hot plumes, in the depth range from 20 to 30 km (i.e., in the lower crust). These plumes (imaged in the S-velocities of the present model) are consistent with the elevated heat flow [25] and the hydrothermal activity [62] that exist in this area. These plumes are produced by a partial-melting asthenospheric diapir, discovered in the upper mantle by Rodnikov et al. [63, 64]. The low S velocities determined beneath the volcanic belt of the KP, for both upper and lower crust, are in agreement with the abundant volcanic activity existing in this area [9]. For the SO, the crustal thickness determined in the present study (Figure 3(a)) tallies with that calculated by Rodnikov et al. [25]. In general, the Moho map shown in Figure 3(a) is in agreement with that obtained by other authors [7, 31]. The crustal thickness of the SO is considered by Zeng and Lay [29] as an intermediate thick crust, probably a thin continental thickened by subcrustal flow, by deformation or by some process of underplating. For the KB, the Moho depth is determined at 11–13 km by Galperin and Kosminskaya [33]. Their thin crust tallies well with that determined in the present study (Figure 3(a)), which is considered a thinned continental crust by Baranov et al. [32], as testified by their isotopic analysis Sr-Nd-Pb of volcanic rocks. However, Khain [34] consider that the KB is a back arc basin, in which a suboceanic crust associated with arc-rear spreading is assumed. Also, the KB is also assumed as an oceanic basin by others authors [35, 65, 66], considering principally the crustal thickness of this basin.

5.3. Depth Range: 35–60 km. The S-wave velocity shows that the SO and the major southern part of the KP lie on a common plate: the Okhotsk plate [16], because similar S velocities are displayed in all study area (e.g., Figures 2(b) and 2(c)). The difference in S-wave velocity values that can be observed in all this area is associated to its different tectonic features (principally: different age regions, presence of partial melting, the volcanic belt in the KP, and the wedge associated to the Pacific subduction slab), and they are not associated to the existence of different plates. For the SO, the conspicuous low S-wave velocity determined at the southwest (Figure 2(b) and Supplement 15) tallies with a

high conductivity layer determined by Lyapishev et al. [67], in the depth range from 30 to 65 km, which nature can be related to partial melting [25]. Also, this low S-wave velocity is in agreement with deep temperatures in the upper mantle, seismic research, and other geophysical data (e.g., [23, 68]). The low S velocities determined near to the Kuril arc (and along it) show the presence of the wedge associated to the Pacific subducting slab. For the KP, the low S-wave velocity pattern determined beneath the volcanic belt is clearly defined from the upper crust (~5 km-depth) down to a depth of ~60 for the southern part of the volcanic belt (Figure 2(b) and profile AA' of Figure 4) and down to a depth of ~140 km for the northern part (Figure 2(c) and profile BB' of Figure 4). In this area, it is observed that the number of earthquakes decreases drastically, and an anomalous electrical conductivity is identified from magnetotelluric sounding data [54]. Moroz and Nurmukhamedov [69] suppose that it is due to a high fluid saturation of the upper mantle, which may feed the active volcanoes of the volcanic belt. This low S-wave velocity pattern is enlarged in size at the northwest (north of ~55°N), following the location of the Kliuchevskoi and Sheveluch volcanoes, confirming that these volcanoes must be a part of the same subduction-induced volcanic process [9], and not back arc volcanoes as suggested by Tatsumi et al. [49].

5.4. Depth Range: 60–240 km. The LAB and the ABB (Figures 3(b) and 3(c), respectively) are in agreement with previous values of lithosphere and asthenosphere thickness obtained by other authors [6, 7, 25, 54]. For the SO, the location and thickness of the asthenosphere (determined in the present study) are both the expected for this region, because the SO is considered a part of a geological block (the Cenozoic marginal sea basin) characterized by thin lithosphere and thick asthenosphere.

5.5. Depth Range: 240–350 km. For the SO, the high S-wave velocity area (Figures 2(c) and 2(d)) associated to the slab (near to the Kuril arc) increases in size gradually from north to south, because the dip angle of this slab decreases gradually southwards, from ~50 degree near southern Kamchatka to ~30 degree under Hokkaido in northern Japan [13, 23, 28, 70]. For the KP, the present S-wave velocity mapping (Figures 2(c), 2(d), and 4) shows that no relict slab underlies the extinct northern Kamchatka volcanic arc, as suggested by Levin et al. [42]. They suggested two episodes of slab loss under northern Kamchatka, but their model is limited to 200 km depth, i.e., their model has not enough depth to reveal the detached slab. Also, the S-wave velocity mapping (Figure 4 and Supplement 15) shows that the slab shoals towards north. Lees et al. [12] considered the thermal ablating related to asthenosphere as the cause of this feature. The present 3D S-wave velocity model (Supplement 15) supports the hypothesis proposed by Jiang et al. [11], in which there exists a gap associated with the loss of the slab beneath Sheveluch and Kliuchevskoi volcanoes, near the northern part of this slab, because no high S-wave velocity associated to this slab is determined for depths greater than 240 km (profile BB', Figure 4). Then, the asthenospheric flow would pass

through the gap to the northwest, around the north slab edge. The low S-wave velocity pattern observed at northwest of the slab edge, confirms the presence this asthenospheric flow (Figures 2(b) and 2(c), and profile BB' of Figure 4). The loss of slab is a feature already observed in other slab edges (e. g., [47, 71, 72]).

6. Conclusions

The principal geological and tectonics features, present in the study area, have been imaged in a high-resolution 3D S-wave velocity model (from 0 to 350 km depth), for the first time. These features are summarized as follows:

- (1) In the depth range from 0 to 5 km: low S-velocities are determined for areas in which are present large sedimentary basins, with thick sedimentary cover
- (2) In the depth range from 5 to 35 km: the low S-velocities determined at the northwest of the SO (from 20 to 30 km depth) are associated to the presence of two lower crust hot plumes, and the low S-velocities determined at the eastern part of the KP (from 5 to 35 km-depth) are associated to its volcanic belt. On the other hand, the high S-velocities are associated to the regions with thinner crustal thickness (as the KB), influenced by the near mantle materials
- (3) In the depth range from 35 to 60 km: the present 3D S-wave velocity model shows that the SO and the major southern part of the KP lie on a common plate (the Okhotsk plate), because the different S-wave velocity values determined in the study area are not associated to the existence of different plates, but to the tectonic features present in this area. For the SO, the higher S-wave velocity values are associated to the older regions, which is more evident for the Okhotsk Arch. A conspicuous low S-wave velocity is determined at the southwest (from 35 to 60 km depth), which tallies with a high conductivity layer previously determined from 30 to 65 km depth, with deep temperatures in the upper mantle, seismic research, and other geophysical data. The low S-velocities observed near to the Kuril arc (and along it) show the presence of the wedge associated to the Pacific subducting slab. For the KP, low S-velocities are determined beneath the volcanic belt, in the same area as in the previous depth range. This low S-wave velocity pattern is clearly defined from the upper crust (~5 km-depth) down to a depth of ~60 for the southern part of the volcanic belt and down to a depth of ~140 km for the northern part. This low S-wave velocity pattern is enlarged in size at the northwest (north of ~55°N), following the location of the Kliuchevskoi and Sheveluch volcanoes, which confirms that these volcanoes must be a part of the same subduction-induced volcanic process
- (4) In the depth range from 60 to 240 km: the asthenosphere is mapped as low S velocities between the LAB and the ABB. The precise location and detailed structure of the asthenosphere determined in the present study is a new feature that has not been determined in other previous studies. For the SO, the location and thickness of the asthenosphere both coincide with the expected for this area, which is part of a geological block (the Cenozoic marginal sea basin) that is characterized by thin lithosphere and thick asthenosphere. The subducting Pacific slab (for the SO and the KP) is shown as a high S-wave velocity pattern, and its corresponding wedge (above this slab) is shown as a low S-wave velocity pattern
- (5) In the depth range from 240 to 350 km: the high S-wave velocity area associated to the slab (near to the Kuril arc) increases in size gradually from north to south, as the dip angle of this slab decreases. For the KP, the present 3D S-wave velocity model shows that the subducting slab terminates near to the Aleutian-Kamchatka junction, i.e., no relict slab underlies the extinct northern Kamchatka volcanic arc. This model shows that the slab shoals towards north, and there exists a gap associated with the loss of this slab beneath Sheveluch and Kliuchevskoi volcanoes. The low S-wave velocity pattern observed at northwest of the slab edge confirms the presence of the asthenospheric flow, which would pass through the gap to the northwest around the north slab edge

Data Availability

Datasets for this research are available in the National Geophysical Data Center (from the web server at <https://maps.ngdc.noaa.gov/viewers/grid-extract/index.html>) and in the Incorporated Research Institutions for Seismology (from the web server at http://www.iris.washington.edu/wilber3/find_event).

Conflicts of Interest

The author declares to have no potential conflicts of interest.

Acknowledgments

For this study, the National Geophysical Data Center (NGDC) and the Incorporated Research Institutions for Seismology (IRIS) have provided the elevation and seismic data, respectively. This work was partially supported by a Sciences Research Project of the University of Almería (grant number UAL2020-FQM-B2075).

Supplementary Materials

Supplementary 1. Supplement 1. List of the events used in this study (278 events). The agency according to which has been listed the epicenter coordinates and origin times, is the National Earthquake Information Center (NEIC).

Supplementary 2. Supplement 2. List of the stations used in this study (12 stations).

Supplementary 3. Supplement 3. List of the source zones used in this study (77 source zones).

Supplementary 4. Supplement 4. List of the averaged stations defined in this study (2 new codes).

Supplementary 5. Supplement 5. Steps followed in the filtering process of each event-station seismogram to obtain its dispersion curve [50]. The circles are used to denote the application of a digital filtering technique and the rectangles are used to denote the results obtained. The enhanced rectangles are used to show the initial data and the final result.

Supplementary 6. Supplement 6. (a) Observed seismogram corresponding to the event 267 (Supplement 1) recorded at station MDJ (IC network, Supplement 2), instrument corrected. (b) Contour map of relative energy normalized to 99 decibels, as a function of the period and the group time (white points denote the group times inferred from the energy map). (c) Group time curve inferred from the energy map. (d) Group velocities calculated from the group times and the epicentral distance (group velocity is the epicentral distance divided by the group time for each period).

Supplementary 7. Supplement 7. (a) Observed seismogram corresponding to the event shown in Supplement 6a. (b) Group velocity dispersion curve obtained after application of the MFT (as shown in Supplement 6). (c) Time-variable filtered seismogram.

Supplementary 8. Supplement 8. (a) Time-variable filtered seismogram obtained after application of the TVF, as shown in Supplement 7. (b) Contour map of relative energy normalized to 99 decibels as a function of the period and the group time (white points denote the group times inferred from the energy map). (c) Group time curve inferred from the energy map. (d) Group velocities calculated from the group times and the epicentral distance.

Supplementary 9. Supplement 9. (a) Path coverage of the Rayleigh waves (253 paths). The rectangle plotted with black thick line shows the area considered under study, as shown in Figures 1–3. (b) Number of paths calculated for each dispersion data period determined from the Rayleigh-wave analysis.

Supplementary 10. Supplement 10. Group velocities obtained for the 253 source-station paths considered in this study. The standard deviation (1-sigma error) of the group velocities is for all paths ranging from 0.03 to 0.07 km/s, with a media value of these errors of 0.05 km/s.

Supplementary 11. Supplement 11. Rayleigh-wave group velocity $U(x, y)$, computed by regionalization using Fourier seires. The isolines interval is 0.1 km/s.

Supplementary 12. Supplement 12. Error in the Rayleigh-wave group velocity $\Delta U(x, y)$, arisen in computation of the regionalized velocity $U(x, y)$ shown in Supplement 11. The isolines interval is 0.01 km/s.

Supplementary 13. Supplement 13. Initial earth model (α : P-wave velocity, β : S-wave velocity, and ρ : density) considered for the inversion of the group velocities (obtained by regionalization), for the block area located at the coordinates: 55.375°N, 158.125°E.

Supplementary 14. Supplement 14. (a) Shear-wave velocity (final model) obtained after the inversion process for the block area located at the coordinates: 55.375°N, 158.125°E, plotted with blue line only from 0 to 800 km of depth. The horizontal bars show standard deviation for each layer considered in this inversion process. The shear velocity distribution of the initial model listed in Supplement 13 is plotted with red line, only from 0 to 800 km of depth. (b) Resolving kernels of the inversion problem posed (plotted only from 0 to 800 km of depth). The reference depths are marked by vertical bars for the media depth of each layer considered. (c) The theoretical group velocity obtained from the final model plotted in Supplement 14a, is shown with blue line. The theoretical group velocity obtained from the initial model listed in Supplement 13 (and plotted also in Supplement 14a), by means of forward modelling, is plotted with red line. The dots line denotes the average group velocity, calculated by regionalization, for the above-mentioned block area (considered as observed data). The vertical bars show the standard deviation in group velocities at each period (1- σ errors in the observed data).

Supplementary 15. Supplement 15. Geographical distribution of the S-wave velocity as a function of depth. The interval between isolines is 0.1 km/s.

Supplementary 16. Supplement 16. Geographical distribution of the 1-sigma errors arisen in computation of the S-velocities shown in Supplement 15. The interval between isolines is 0.01 km/s.

Supplementary 17. Supplement 17. Resolution maps of the inversion process performed to calculate the S-velocities shown in Supplement 15, plotted from 0 (not resolved) to 1 (perfect resolution). The interval between isolines is 0.1.

References

- [1] E. Bourova, K. Yoshizawa, and K. Yomogida, "Upper mantle structure of marginal seas and subduction zones in northeastern Eurasia from Rayleigh wave tomography," *Physics of the Earth and Planetary Interiors*, vol. 183, no. 1-2, pp. 20–32, 2010.
- [2] C. P. Legendre, L. Zhao, and Q.-F. Chen, "Upper-mantle shear-wave structure under east and Southeast Asia from automated multimode inversion of waveforms," *Geophysical Journal International*, vol. 203, no. 1, pp. 707–719, 2015.
- [3] M. H. Ritzwoller and A. L. Levshin, "Eurasian surface wave tomography: group velocities," *Journal of Geophysical Research*, vol. 103, no. B3, pp. 4839–4878, 1998.
- [4] N. M. Shapiro, A. V. Gorbatov, E. Gordeev, and J. Dominguez, "Average shear-wave velocity structure of the Kamchatka peninsula from the dispersion of surface waves," *Earth, Planets and Space*, vol. 52, no. 9, pp. 573–577, 2000.
- [5] T. B. Yanovskaya and V. M. Kozhevnikov, "3D S-wave velocity pattern in the upper mantle beneath the continent of Asia

- from Rayleigh wave data,” *Physics of the Earth and Planetary Interiors*, vol. 138, no. 3-4, pp. 263–278, 2003.
- [6] J.-S. Zhu, J.-M. Cao, X.-L. Cai, Z.-Q. Yan, and X.-L. Cao, “High resolution surface wave tomography in East Asia and West Pacific marginal sea,” *Chinese Journal of Geophysics*, vol. 45, no. 5, pp. 679–698, 2002.
- [7] J. Zhu, “The structural characteristics of lithosphere in the continent of Eurasia and its marginal seas,” *Earth Science Frontiers*, vol. 14, no. 3, pp. 1–20, 2007.
- [8] V. Corchete, “Crustal and upper-mantle structure beneath the South China Sea and Indonesia,” *Geological Society of America Bulletin*, vol. 133, pp. 177–184, 2020.
- [9] A. Gorbатов, J. Domínguez, G. Suárez, V. Kostoglodov, D. Zhao, and E. Gordeev, “Tomographic imaging of the P-wave velocity structure beneath the Kamchatka peninsula,” *Geophysical Journal International*, vol. 137, no. 2, pp. 269–279, 1999.
- [10] A. Gorbатов, S. Widiyantoro, Y. Fukao, and E. Gordeev, “Signature of remnant slabs in the North Pacific from P-wave tomography,” *Geophysical Journal International*, vol. 142, no. 1, pp. 27–36, 2000.
- [11] G. Jiang, D. Zhao, and G. Zhang, “Seismic tomography of the Pacific slab edge under Kamchatka,” *Tectonophysics*, vol. 465, no. 1-4, pp. 190–203, 2009.
- [12] J. M. Lees, J. Van Decar, E. Gordeev et al., “Three Ddimensional images of the Kamchatka-Pacific plate cusp,” in *Volcanism and Subduction: The Kamchatka Region Geophysical, Monograph Series 172, Copyright 2007 by the American Geophysical Union*, pp. 65–75, Wiley, 2013.
- [13] M. S. Miller and B. L. N. Kennett, “Evolution of mantle structure beneath the Northwest Pacific: evidence from seismic tomography and paleogeographic reconstructions,” *Tectonics*, vol. 25, no. 4, article TC4002, 2006.
- [14] Y. F. Moroz and L. I. Gontovaya, “Deep structure of Kamchatka according to the results of MT sounding and seismic tomography,” *Russian Journal of Pacific Geology*, vol. 11, no. 5, pp. 354–367, 2017.
- [15] V. Corchete, *Crust and Upper Mantle Structure beneath the Yellow Sea, the East China Sea, the Japan Sea and the Philippine Sea*, Science China, 2020.
- [16] D. B. Cook, K. Fujita, and C. A. McMullen, “Present-day plate interactions in Northeast Asia: North American, Eurasian, and Okhotsk plates,” *Journal of Geodynamics*, vol. 6, no. 1-4, pp. 33–51, 1986.
- [17] L. A. Savostin, A. I. Verzhbitskaya, and B. V. Baranov, “Holocene plate tectonics of the Sea of Okhotsk region,” *Doklady Academy of Sciences, USSR, Earth Sciences Section*, vol. 266, pp. 62–65, 1982.
- [18] L. Savostin, L. Zonenshain, and B. Baranov, “Geology and plate tectonics of the Sea of Okhotsk,” *American Geophysical Union, Geodynamics Series*, vol. 11, pp. 189–221, 1983.
- [19] T. Seno, T. Sakurai, and S. Stein, “Can the Okhotsk plate be discriminated from the North American plate?,” *Journal of Geophysical Research*, vol. 101, no. B5, pp. 11305–11315, 1996.
- [20] K. Fujita, B. M. Kozmin, K. G. Mackey, S. A. Riegel, M. S. McLean, and V. S. Imaev, “Seismotectonics of the Chersky seismic belt, eastern Sakha Republic (Yakutia) and Magadan District, Russia,” *Stephan Mueller Special Publication Series*, vol. 4, pp. 117–145, 2009.
- [21] D. Hindle, B. Sedov, S. Lindauer, and K. Mackey, “The Ula-khan fault surface rupture and the seismicity of the Okhotsk-North America plate boundary,” *Solid Earth*, vol. 10, no. 2, pp. 561–580, 2019.
- [22] L. Imaeva, G. Gusev, V. Imaev, and V. Melnikova, “Neotectonic activity and parameters of seismotectonic deformations of seismic belts in Northeast Asia,” *Journal of Asian Earth Sciences*, vol. 148, pp. 254–264, 2017.
- [23] I. Y. Koulakov, N. L. Dobretsov, N. A. Bushenkova, and A. V. Yakovlev, “Slab shape in subduction zones beneath the Kurile-Kamchatka and Aleutian arcs based on regional tomography results,” *Russian Geology and Geophysics*, vol. 52, no. 6, pp. 650–667, 2011.
- [24] N. I. Pavlenkova, S. N. Kashubin, T. S. Sakoulina, and G. A. Pavlenkova, “Geodynamic nature of the Okhotsk Sea lithosphere. An overview of seismic constraints,” *Tectonophysics*, vol. 777, article 228320, 2020.
- [25] A. G. Rodnikov, N. A. Sergeeva, L. P. Zabarinskaya, N. I. Filatova, V. P. Piip, and V. A. Rashidov, “The deep structure of active continental margins of the Far East (Russia),” *Russian Journal of Earth Sciences*, vol. 10, no. 4, pp. 1–23, 2008.
- [26] C. Li, G. Zhang, X. Wang, Z. Wang, and J. Fang, “Three-dimensional lithospheric density distribution of China and surrounding regions,” *Geoscience Frontiers*, vol. 5, no. 1, pp. 95–102, 2014.
- [27] L.-B. Zhu, Q. Xu, and X.-F. Chen, “Group velocity Rayleigh wave in Chinese continent and its adjacent seas,” *Chinese Journal of Geophysics*, vol. 45, no. 4, pp. 491–501, 2002.
- [28] D. Zhao, F. Pirajno, N. L. Dobretsov, and L. Liu, “Mantle structure and dynamics under East Russia and adjacent regions,” *Russian Geology and Geophysics*, vol. 51, no. 9, pp. 925–938, 2010.
- [29] Y. Zheng and T. Lay, “Low Vp/Vs ratios in the crust and upper mantle beneath the Sea of Okhotsk inferred from teleseismic $p_M p$, $s_M p$, and $s_M s$ underside reflections from the Moho,” *Journal of Geophysical Research*, vol. 111, no. B1, article B01305, 2006.
- [30] N. I. Christensen and W. D. Mooney, “Seismic velocity structure and composition of the continental crust: a global view,” *Journal of Geophysical Research*, vol. 100, no. B6, pp. 9761–9788, 1995.
- [31] H. S. Gnidbenko and I. I. Khvedchuk, “The tectonics of the Okhotsk Sea,” *Marine Geology*, vol. 50, no. 3, pp. 155–197, 1982.
- [32] B. Baranov, K. Dozorova, B. Karp, and V. Karnaukh, “The geometry of Kuril Basin opening,” *DAN*, vol. 367, no. 3, p. 376, 1999.
- [33] E. I. Galperin and I. P. Kosminskaya, Eds., *Structure of the Crust in the Transition Zone from the Asian Continent to the Pacific Ocean*, Nauka, Moscow, Russia, 1964.
- [34] V. E. Khain, *Tectonics of Continents and Oceans (2000)*, Nauchnyi mir, Moscow, Russia, 2001.
- [35] S. N. Kashubin, O. V. Petrov, A. V. Rybalka et al., “Earth’s crust model of the south-Okhotsk Basin by wide-angle OBS data,” *Tectonophysics*, vol. 710-711, pp. 37–55, 2017.
- [36] C. DeMets, R. G. Gordon, D. F. Argus, and S. Stein, “Current plate motions,” *Geophysical Journal International*, vol. 101, no. 2, pp. 425–478, 1990.
- [37] G. Steblov, M. Kogan, R. King, C. Scholz, R. Bürgmann, and D. Frolov, “Imprint of the North American plate in Siberia revealed by GPS,” *Geophysical Research Letters*, vol. 30, no. 18, article GL017805, 2003.

- [38] A. Gorbatov, V. Kostoglodov, G. Suárez, and E. Gordeev, "Seismicity and structure of the Kamchatka subduction zone," *Journal of Geophysical Research*, vol. 102, no. B8, pp. 17883–17898, 1997.
- [39] T. Cahill and B. L. Isacks, "Seismicity and shape of the subducted Nazca plate," *Journal of Geophysical Research*, vol. 97, no. B12, pp. 17503–17529, 1992.
- [40] M. Pardo and G. Suárez, "Shape of the subducted Rivera and Cocos plates in southern Mexico: seismic and tectonic implications," *Journal of Geophysical Research*, vol. 100, no. B7, pp. 12357–12373, 1995.
- [41] D. K. Rea and R. Stax, "Paleoceanographic record of North Pacific quantified," *Eos*, vol. 74, no. 36, pp. 406–411, 1993.
- [42] V. Levin, N. Shapiro, J. Park, and M. Ritzwoller, "Seismic evidence for catastrophic slab loss beneath Kamchatka," *Nature*, vol. 418, no. 6899, pp. 763–767, 2002.
- [43] G. M. Yogodzinski, J. M. Lees, T. G. Churikova, F. Dorendorf, G. Wöerner, and O. N. Volynets, "Geochemical evidence for the melting of subducting oceanic lithosphere at plate edges," *Nature*, vol. 409, no. 6819, pp. 500–504, 2001.
- [44] J. Park, V. Levin, M. Brandon et al., "A dangling slab, amplified arc volcanism, mantle flow and seismic anisotropy in the Kamchatka plate corner," in *AGU Geodynamics Series, 30, Plate Boundary Zones*, S. Stein and J. T. Freymueller, Eds., pp. 295–324, Wiley, 2002.
- [45] V. Peyton, V. Levin, J. Park et al., "Mantle flow at a slab edge: seismic anisotropy in the Kamchatka region," *Geophysical Research Letters*, vol. 28, no. 2, pp. 379–382, 2001.
- [46] M. Portnyagin, K. Hoernle, G. Avdeiko et al., "Transition from arc to oceanic magmatism at the Kamchatka-Aleutian junction," *Geology*, vol. 33, no. 1, pp. 25–28, 2005.
- [47] M. J. R. Wortel and W. Spakman, "Subduction and slab detachment in the Mediterranean-Carpathian region," *Science*, vol. 290, no. 5498, pp. 1910–1917, 2000.
- [48] A. Davaille and M. Lees, "Thermal modeling of subducted plates: tear and hotspot at the Kamchatka corner," *Earth Planetary Science Letters*, vol. 226, no. 3-4, pp. 293–304, 2004.
- [49] Y. Tatsumi, Y. Furukawa, T. Kogiso, Y. Yamanaka, T. Yokoyama, and S. Fedotov, "A third volcanic chain in Kamchatka: thermal anomaly at transform/convergence plate boundary," *Geophysical Research Letters*, vol. 21, no. 7, pp. 537–540, 1994.
- [50] V. Corchete, M. Chourak, and H. M. Hussein, "Shear wave velocity structure of the Sinai Peninsula from Rayleigh wave analysis," *Surveys in Geophysics*, vol. 28, no. 4, pp. 299–324, 2007.
- [51] V. Corchete, "Shear-wave velocity structure of Australia from Rayleigh-wave analysis," *Earth Science Research Journal*, vol. 18, pp. 87–98, 2015.
- [52] V. Corchete, "Crustal and upper mantle structure beneath the Gulf of Mexico and the Caribbean Sea from Rayleigh-wave analysis," *Geological Journal*, vol. 53, no. 5, pp. 1743–1754, 2018.
- [53] A. M. Dziewonski and D. L. Anderson, "Preliminary reference earth model," *Physics of the Earth and Planetary Interiors*, vol. 25, no. 4, pp. 297–356, 1981.
- [54] I. V. Nizkous, I. A. Sanina, E. Kissling, and L. I. Gontovaya, "Velocity properties of the lithosphere in the ocean-continent transition zone in the Kamchatka region from seismic tomography data," *Izvestiya, Physics of the Solid Earth*, vol. 42, no. 4, pp. 286–296, 2006.
- [55] Y. F. Moroz, "On deep structure of East Kamchatka according to magnetotelluric sounding," *Volcanic Seismology*, vol. 5, pp. 85–90, 1984.
- [56] V. P. Zinkevich, "Structural zonation of eastern Kamchatka and characteristic features of its deep-seated structure," in *Accretional Tectonics of Eastern Kamchatka*, Y. M. Pusharovskiy, Ed., pp. 16–27, Nauka, Moscow, Russia, 1993.
- [57] S. K. Bikkenina, G. I. Anosov, V. V. Argentov, and K. F. Sergeev, *Crustal Structure of the Southern Okhotsk Sea according to Seismic Refraction Data*, Nauka, Moscow, Russia, 1987.
- [58] V. G. Prokudin, "On the age of the sedimentary cover of the Kurile Basin, Sea of Okhotsk," *Russian Journal of Pacific Geology*, vol. 9, no. 3, pp. 215–226, 2015.
- [59] E. P. Terekhov, I. B. Tsoy, N. G. Vashchenkova, A. V. Mozherovskii, and M. T. Gorovaya, "Sedimentation settings and evolution history of the Kuril Basin (Sea of Okhotsk) in the Cenozoic," *Oceanology*, vol. 48, no. 4, pp. 569–577, 2008.
- [60] I. Koulakov, A. S. Serdyukov, A. V. Kononov et al., "Possible sources of hydrothermal activity and mud volcanism in southern Sakhalin inferred from local earthquake seismic tomography," *Geochemistry Geophysics Geosystems*, vol. 18, no. 5, pp. 1943–1958, 2017.
- [61] K.-S. Wang, X.-F. Shi, J.-J. Zou et al., "Sediment provenance variations in the southern Okhotsk Sea over the last 180 ka: evidence from light and heavy minerals," *Palaeogeography Palaeoclimatology Palaeoecology*, vol. 479, pp. 61–70, 2017.
- [62] V. B. Piip and A. G. Rodnikov, "The Sea of Okhotsk crust from deep seismic sounding data," *Russian Journal of Earth Sciences*, vol. 6, no. 1, pp. 35–48, 2004.
- [63] A. G. Rodnikov, N. A. Sergeeva, and L. P. Zabarinskaya, "Deep crustal structure of sedimentary basins in the transition zone from Asia to the Pacific Ocean," in *Geophysics of the XXI Century*, pp. 102–111, GEON, "Nauchnyi Mir", 2001.
- [64] A. G. Rodnikov, N. A. Sergeeva, and L. P. Zabarinskaya, "Deep structure of the Eurasia-Pacific transition zone," *Russian Journal of Earth Sciences*, vol. 3, no. 4, pp. 293–310, 2001.
- [65] S. N. Kashubin, Y. Lukashin, T. S. Sakoulina, and N. I. Pavlenkova, "Modern methods of conducting and interpretation of deep seismic sounding in the marginal seas of Russia," in *Relevance of G. A. Gamburtsev's Ideas in the XXI Century*, pp. 175–194, Nauka, Moscow, Russia, 2013.
- [66] N. I. Pavlenkova, V. N. Pilipenko, A. O. Verpakhovskaja, G. A. Pavlenkova, and V. P. Filonenko, "Crustal structure in Chile and Okhotsk Sea regions," *Tectonophysics*, vol. 472, no. 1-4, pp. 28–38, 2009.
- [67] A. M. Lyapishev, P. M. Sychev, and V. Y. Semenov, "The structure of electrical conduction of the upper mantle of the Kuril Basin of the Sea of Okhotsk," *Tikhookeanskaya Geologia*, vol. 4, p. 45, 1987.
- [68] S. Maruyama, Y. Isozaki, J. Kimura, and M. Terabayashi, "Pacific-type orogeny revisited: Miyashiro-type orogeny proposed," *The Island Arc*, vol. 6, no. 1, pp. 91–120, 1997.
- [69] Y. F. Moroz and A. G. Nurmukhamedov, "A deep geoelectric model of the junction zone of the Kurile-Kamchatka and Aleutian Island arcs," *Izvestiya, Physics of the Solid Earth*, vol. 40, pp. 502–514, 2004.

- [70] N. Schmerr and C. Thomas, "Subducted lithosphere beneath the Kuriles from migration of PP precursors," *Earth and Planetary Science Letters*, vol. 311, no. 1-2, pp. 101-111, 2011.
- [71] S. E. Lallemand, Y. Font, H. Bijwaard, and H. Kao, "New insights on 3-D plates interaction near Taiwan from tomography and tectonic implications," *Tectonophysics*, vol. 335, no. 3-4, pp. 229-253, 2001.
- [72] F. P. Lucente, C. Chiarabba, G. B. Cimini, and D. Giardini, "Tomographic constraints on the geodynamic evolution of the Italian region," *Journal of Geophysical Research*, vol. 104, no. B9, pp. 20307-20327, 1999.